6th European Conference on Computational Mechanics (ECCM 6)
7th European Conference on Computational Fluid Dynamics (ECFD 7)
1115 June 2018, Glasgow, UK

A DISCONTINUOUS GALERKIN FORMULATION FOR VARIABLE ANGLE TOW COMPOSITE PLATES HIGHER-ORDER THEORIES

V. GULIZZI[1], I. BENEDETTI[2] AND A. MILAZZO[3]

[1] DICAM, Università degli Studi di Palermo
Viale delle Scienze, 90128 Palermo, Italy
vincenzo.gulizzi@unipa.it, http://www.unipa.it/persone/docenti/g/vincenzo.gulizzi

[2] DICAM, Università degli Studi di Palermo
Viale delle Scienze, 90128 Palermo, Italy
ivano.benedetti@unipa.it, http://www.unipa.it/persone/docenti/b/ivano.benedetti

[3] DICAM, Università degli Studi di Palermo
Viale delle Scienze, 90128 Palermo, Italy
alberto.milazzo@unipa.it, http://www.unipa.it/persone/docenti/m/alberto.milazzo

Key words: Variable angle tow composites, multi-layered plates, higher order theories, Discontinuous Galerkin methods

Abstract. A discontinuous Galerkin formulation for the mechanical behaviour of Variable Angle Tow multi-layered composite plates is presented. The starting point of the formulation is the strong form of the governing equations, which are obtained by means of the Principle of Virtual Displacement, the Generalized Unified Formulation and the Equivalent Single Layer assumption for the mechanical behaviour of the whole assembly. To obtain the corresponding discontinuous Galerkin formulation, an auxiliary flux variable is introduced and the governing equations are rewritten as a first-order system of partial differential equations. To link neighbouring mesh elements, suitably defined numerical fluxes are introduced and an Interior Penalty discontinuous Galerkin formulation is obtained and presented. *hp*-convergence analyses for straight-fiber composite plates and a comparison with the results available in the literature for variable angle tow plates show the accuracy of the proposed formulation as well as the computational savings in terms of overall degrees of freedom.

1 INTRODUCTION

Classically, laminated fiber-reinforced composite plates are made of a sequence of layers of unidirectional long fibers, which are conveniently oriented, stacked and bonded together to obtain one or more desired properties in the final assembly [1]. The current advancements in materials manufacturing, and more specifically in fiber placement technology, now allow to spatially control and continuously vary the orientation of the fibers within

each layer of the laminate. Laminated composite structures obtained by employing this process are referred to as Variable Angle Tow (VAT) composite structures. VAT composite plates have shown superior mechanical properties in terms of static response [2], buckling and post-buckling behavior [3, 4, 5], thanks to the possibility to optimize the spatial variation of the fibers [6] alongside the stacking sequence and the layers' thickness. However, despite the enhanced flexibility in terms of design parameters, VAT composites display an inherent in-plane variable and through-the-thickness heterogeneous structure. Therefore, their analysis and design are generally more complex than straight-fiber composites and generally require the aid of numerical models.

In this work, a discontinuous Galerkin (dG) formulation for the mechanical behaviour of VAT composite plates is presented. With respect to classical finite element approaches, dG formulations have the advantage of being more flexible when complex geometries are considered and/or when hierarchical meshes are needed [7]. The formulation is based on the strong form of the governing equations for VAT plates, which are obtained starting from the Principle of Virtual Displacement (PVD) for each layer [8, 9] and adopting the Generalized Unified Formulation (GUF) in combination with the Equivalent Single Layer (ESL) assumption for the through-the-thickness behavior of the plate assembly [10, 11]. Following Arnold et al. [12], the corresponding dG formulation is obtained by defining an auxiliary flux variable and by rewriting the governing equations as a first-order system of partial differential equations, which are then stated in weak sense over each mesh element. By introducing suitably defined numerical fluxes at the boundary of the mesh elements, the numerical model for the whole plate domain is retrieved and an Interior Penalty (IP) discontinuous Galerkin formulation is obtained and discussed.

The proposed formulation is first tested with straight-fiber composite plates and the results of the *hp*-convergence analyses on a Cartesian grid allow to assess the accuracy of the approach for a specific selection of the penalty parameters. Then the formulation is employed to compute the mechanical response of a variable angle tow composite plate and the results are compared with those available in the literature showing a satisfactory accuracy as well as noticeable savings in terms of degrees of freedom of the overall system.

2 BOUNDARY VALUE PROBLEM

Let us consider a generic VAT composite plate referred to a global reference system $x_1x_2x_3$ as shown in Fig.(1). The plate occupies the domain V and its boundary is denoted by $\partial V \equiv S = S_l \cup S_t \cup S_b$, where S_l is the lateral surface of the plate and S_t and S_b are the top and bottom surfaces, which are assumed to lie parallel to the x_1x_2 plane at the heights $x_3 = \tau_t$ and $x_3 = \tau_b$, respectively. It follows that the thickness τ of the plate is $\tau = \tau_t - \tau_b$. The plate consists of N_ℓ VAT layers and the generic ℓ-th layer is identified by the bottom and top faces lying at the heights $x_3 = \tau_t^{\langle \ell \rangle}$ and $x_3 = \tau_b^{\langle \ell \rangle}$, respectively. The layers are stacked in such a way that $\tau_t^{\langle \ell-1 \rangle} = \tau_b^{\langle \ell \rangle}$, $\forall \ell = 2, \dots, N_\ell$. Moreover, the ℓ-th VAT layer is characterized by a fiber orientation $\theta^{\langle \ell \rangle}$ that is a function of the spatial coordinates x_1 and x_2, i.e. $\theta^{\langle \ell \rangle} = \theta^{\langle \ell \rangle}(x_1, x_2)$, which leads to a specific layer's constitutive behavior as discussed in Sec.(2.1).

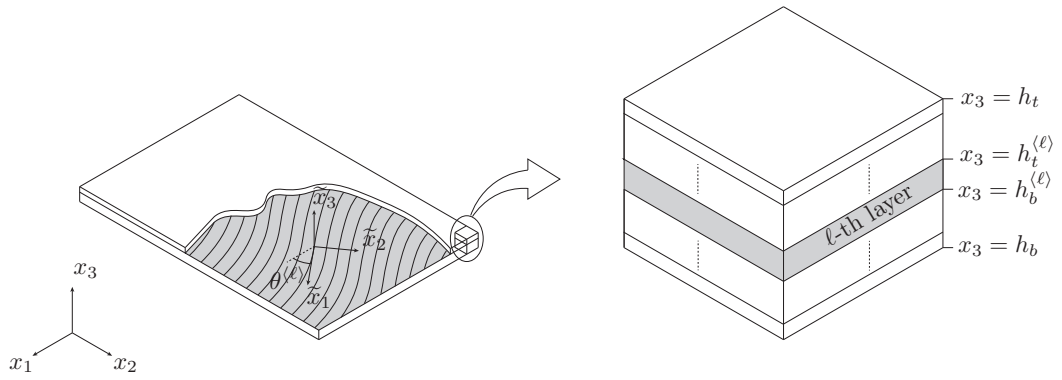

Figure 1: Schematic representation of a laminated composite plate made of VAT layers.

In the next sections, $\boldsymbol{u} = \{u_1, u_2, u_3\}$, $\boldsymbol{b} = \{b_1, b_2, b_3\}$, $\boldsymbol{t} = \{t_1, t_2, t_3\}$ denote the displacements field, the volume forces and the surface tractions, respectively, and $\boldsymbol{\gamma} = \{\gamma_{11}, \gamma_{22}, \gamma_{33}, \gamma_{23}, \gamma_{13}, \gamma_{12}\}$ and $\boldsymbol{\sigma} = \{\sigma_{11}, \sigma_{22}, \sigma_{33}, \sigma_{23}, \sigma_{13}, \sigma_{12}\}$ denote the strain and the stress fields in Voigt notation, respectively. Moreover, quantities referred to the ℓ-th layer will be denoted using the superscript $\langle\ell\rangle$.

2.1 VAT layer's constitutive behavior

The generic ℓ-th layer of the VAT plate is assumed to be made of a linear elastic material, whose mechanical properties continuously vary as a function of the spatial variables x_1 and x_2 in terms of the local orientation of the fibers $\theta^{\langle\ell\rangle}(x_1, x_2)$, which defines a local reference system $\widetilde{x}_1\widetilde{x}_2\widetilde{x}_3$ as shown in Fig.(1). It is worth underlining that the $\widetilde{x}_3$ direction of $\widetilde{x}_1\widetilde{x}_2\widetilde{x}_3$ is aligned with the x_3 direction of the plate reference system. In this local reference system, the layer's material is assumed to be orthotropic and the stress-strain relation is modelled using the relation $\widetilde{\boldsymbol{\sigma}}^{\langle\ell\rangle} = \widetilde{\boldsymbol{c}}^{\langle\ell\rangle}\widetilde{\boldsymbol{\gamma}}^{\langle\ell\rangle}$, where $\widetilde{\boldsymbol{c}}^{\langle\ell\rangle}$ is the 6×6 elasticity coefficients matrix. When referred to the plate reference system $x_1x_2x_3$, the stress-strain relationship becomes

$$\boldsymbol{\sigma}^{\langle\ell\rangle} = \boldsymbol{c}^{\langle\ell\rangle}\boldsymbol{\gamma}^{\langle\ell\rangle}, \tag{1}$$

where $\boldsymbol{\sigma}^{\langle\ell\rangle} = \boldsymbol{T}_\sigma^{-1}(\theta^{\langle\ell\rangle})\widetilde{\boldsymbol{\sigma}}^{\langle\ell\rangle}$, $\boldsymbol{\gamma}^{\langle\ell\rangle} = \boldsymbol{T}_\gamma^{-1}(\theta^{\langle\ell\rangle})\widetilde{\boldsymbol{\gamma}}^{\langle\ell\rangle}$, $\boldsymbol{c}^{\langle\ell\rangle} = \boldsymbol{T}_\sigma^{-1}(\theta^{\langle\ell\rangle})\widetilde{\boldsymbol{c}}^{\langle\ell\rangle}\boldsymbol{T}_\gamma(\theta^{\langle\ell\rangle})$ and $\boldsymbol{T}_\sigma(\theta^{\langle\ell\rangle})$ and $\boldsymbol{T}_\gamma(\theta^{\langle\ell\rangle})$ are suitably defined transformation matrices [1] that in this case depend on the spatial position given by x_1 and x_2.

2.2 Generalized unified theories for VAT composite plates

In this work, assuming small strains, the strain-displacements relationship are written by separating the derivatives with respect to x_1 and x_2 and the derivative with respect to

x_3 as follows

$$\boldsymbol{\gamma}^{\langle\ell\rangle} = \boldsymbol{I}_1 \frac{\partial \boldsymbol{u}^{\langle\ell\rangle}}{\partial x_1} + \boldsymbol{I}_2 \frac{\partial \boldsymbol{u}^{\langle\ell\rangle}}{\partial x_2} + \boldsymbol{I}_3 \frac{\partial \boldsymbol{u}^{\langle\ell\rangle}}{\partial x_3} = \boldsymbol{I}_\lambda \frac{\partial \boldsymbol{u}^{\langle\ell\rangle}}{\partial x_\lambda} + \boldsymbol{I}_3 \frac{\partial \boldsymbol{u}^{\langle\ell\rangle}}{\partial x_3}, \tag{2}$$

where the last equality is obtained by considering the Einstein summation convention for the subscript $\lambda = 1, 2$, and the following matrices have been introduced

$$\boldsymbol{I}_1 \equiv \begin{bmatrix} 1 & 0 & 0 \\ 0 & 0 & 0 \\ 0 & 0 & 0 \\ 0 & 0 & 0 \\ 0 & 0 & 1 \\ 0 & 1 & 0 \end{bmatrix}, \quad \boldsymbol{I}_2 \equiv \begin{bmatrix} 0 & 0 & 0 \\ 0 & 1 & 0 \\ 0 & 0 & 0 \\ 0 & 0 & 1 \\ 0 & 0 & 0 \\ 1 & 0 & 0 \end{bmatrix} \quad \text{and} \quad \boldsymbol{I}_3 \equiv \begin{bmatrix} 0 & 0 & 0 \\ 0 & 0 & 0 \\ 0 & 0 & 1 \\ 0 & 1 & 0 \\ 1 & 0 & 0 \\ 0 & 0 & 0 \end{bmatrix}. \tag{3}$$

The variational statement of the Principle of Virtual Displacement for the plate assembly is written as

$$\sum_{\ell=1}^{N_\ell} \int_{V^{\langle\ell\rangle}} \delta\boldsymbol{\gamma}^{\langle\ell\rangle\intercal} \boldsymbol{\sigma}^{\langle\ell\rangle} = \sum_{\ell=1}^{N_\ell} \int_{V^{\langle\ell\rangle}} \delta\boldsymbol{u}^{\langle\ell\rangle\intercal} \boldsymbol{b}^{\langle\ell\rangle} + \sum_{\ell=1}^{N_\ell} \int_{\partial V^{\langle\ell\rangle}} \delta\boldsymbol{u}^{\langle\ell\rangle\intercal} \boldsymbol{t}^{\langle\ell\rangle}, \tag{4}$$

where, in order to underline the functional dependence of the involved quantities, it is assumed that $\boldsymbol{\gamma}^{\langle\ell\rangle} = \boldsymbol{\gamma}(\boldsymbol{u}^{\langle\ell\rangle})$ by means of Eq.(2) and $\boldsymbol{\sigma}^{\langle\ell\rangle} = \boldsymbol{\sigma}(\boldsymbol{\gamma}^{\langle\ell\rangle}(\boldsymbol{u}^{\langle\ell\rangle}))$ by means of Eq.(1). In Eq.(4) and for the remaining part of this work, the differential indicating the measure of integration is dropped as it is clear by means of the domain of integration.

Within the framework of generalized higher order theories for plates, the displacement field $\boldsymbol{u}^{\langle\ell\rangle}$ of each layer is assumed to be expressed as an expansion of products between *unknown* in-plane functions and *known* through-the-thickness functions. Following Carrera [9] and Demasi [10, 11], each component $u_i^{\langle\ell\rangle}$, with $i = 1, 2, 3$, is written using the following series

$$u_i^{\langle\ell\rangle} = u_i^{\langle\ell\rangle}(x_1, x_2, x_3) = \sum_{\alpha=0}^{N_{u_i}} u_{i,\alpha}(x_1, x_2) f_\alpha(x_3), \quad i = 1, 2, 3, \quad \ell = 1, \ldots, N_\ell, \tag{5}$$

where $f_\alpha(x_3)$ denotes the through-the-thickness functions, $u_{i,\alpha}(x_1, x_2)$ denotes the in-plane functions and $N_{u_i} + 1$ is the number of functions for the thickness expansion of u_i. It follows that the total number of introduced unknown functions is $N_u = N_{u_1} + N_{u_2} + N_{u_3} + 3$. In accordance with the Equivalent Single Layer approach, Eq.(5) is assumed to be valid for all the layers of the composite plate, that is the through-the-thickness functions and the in-plane functions are the same for each layer. Interestingly, it is possible to see that Eq.(5) can also be written in matricial form as follows

$$\boldsymbol{u}^{\langle\ell\rangle} = \boldsymbol{F}(x_3)\boldsymbol{U}(x_1, x_2), \quad \ell = 1, \ldots, N_\ell, \tag{6}$$

where $\boldsymbol{U}$ is a $N_u \times 1$ vector collecting the in-plane functions and, consistently, $\boldsymbol{F}$ is a $3 \times N_u$ matrix collecting the through-the-thickness functions. It is worth noting that the

expression given in Eq.(6) does not force to use the same number of expansion terms for the three components of displacement. As an example, in the First Shear Deformation Theory (FSDT) where the displacement components u_1 and u_2 are expanded up to the first order with $f_0 = 1$ and $f_1 = x_3$, and the displacement component u_3 is considered constant throughout the thickness, the matrix $\boldsymbol{F}$ would be

$$\boldsymbol{F} = \begin{bmatrix} 1 & 0 & 0 & x_3 & 0 \\ 0 & 1 & 0 & 0 & x_3 \\ 0 & 0 & 1 & 0 & 0 \end{bmatrix}$$

and the vector $\boldsymbol{U}$ would be $\boldsymbol{U} = \{u, v, w, \theta_y, \theta_x\}$ where u, v and w are the displacement components of the plate mid-plane and θ_y and θ_x are the rotations with respect to the x_2 and x_1 axes, respectively.

Upon substituting Eqs.(6), (2) and (1) into Eq.(4) and integrating along the thickness, one obtains the following expression of the PVD

$$\int_\Omega \frac{\partial \delta \boldsymbol{U}^\intercal}{\partial x_\lambda} \left(\boldsymbol{Q}_{\lambda\mu} \frac{\partial \boldsymbol{U}}{\partial x_\mu} + \boldsymbol{R}_{\lambda 3} \boldsymbol{U} \right) + \delta \boldsymbol{U}^\intercal \left(\boldsymbol{R}_{\lambda 3}^\intercal \frac{\partial \boldsymbol{U}}{\partial x_\lambda} + \boldsymbol{S}_{33} \boldsymbol{U} \right) = \int_\Omega \delta \boldsymbol{U}^\intercal \overline{\boldsymbol{B}} + \int_{\partial\Omega} \delta \boldsymbol{U}^\intercal \boldsymbol{T}, \quad (7)$$

where: Ω is the modeling plane of the plate spanned by the coordinates x_1 and x_2 and $\partial\Omega$ is its boundary; the Einstein summation convention is used for the subscripts λ and μ that take value 1 and 2 only; the matrices $\boldsymbol{Q}_{\lambda\mu}$, $\boldsymbol{R}_{\lambda 3}$ and $\boldsymbol{S}_{33}$ are defined as

$$\boldsymbol{Q}_{\lambda\mu} \equiv \sum_{\ell=1}^{N_\ell} \int_{\tau_b^{\langle\ell\rangle}}^{\tau_t^{\langle\ell\rangle}} \boldsymbol{F}^\intercal \boldsymbol{I}_\lambda^\intercal \boldsymbol{c}^{\langle\ell\rangle} \boldsymbol{I}_\mu \boldsymbol{F}, \quad \boldsymbol{R}_{\lambda 3} \equiv \sum_{\ell=1}^{N_\ell} \int_{\tau_b^{\langle\ell\rangle}}^{\tau_t^{\langle\ell\rangle}} \boldsymbol{F}^\intercal \boldsymbol{I}_\lambda^\intercal \boldsymbol{c}^{\langle\ell\rangle} \boldsymbol{I}_3 \frac{\mathrm{d}\boldsymbol{F}}{\mathrm{d}x_3} \quad (8a)$$

and

$$\boldsymbol{S}_{33} \equiv \int_{\tau_b^{\langle\ell\rangle}}^{\tau_t^{\langle\ell\rangle}} \frac{\mathrm{d}\boldsymbol{F}^\intercal}{\mathrm{d}x_3} \boldsymbol{I}_3^\intercal \boldsymbol{c}^{\langle\ell\rangle} \boldsymbol{I}_3 \frac{\mathrm{d}\boldsymbol{F}}{\mathrm{d}x_3}; \quad (8b)$$

and the vectors $\overline{\boldsymbol{B}}$ and $\boldsymbol{T}$ are defined as

$$\overline{\boldsymbol{B}} \equiv \boldsymbol{F}^\intercal(x_3 = \tau_b)\boldsymbol{t} + \boldsymbol{F}^\intercal(x_3 = \tau_t)\boldsymbol{t} + \sum_{\ell=1}^{N_\ell} \int_{\tau_b^{\langle\ell\rangle}}^{\tau_t^{\langle\ell\rangle}} \boldsymbol{F}^\intercal \boldsymbol{b}^{\langle\ell\rangle} \quad \text{and} \quad \boldsymbol{T} \equiv \sum_{\ell=1}^{N_\ell} \int_{\tau_b^{\langle\ell\rangle}}^{\tau_t^{\langle\ell\rangle}} \boldsymbol{F}^\intercal \boldsymbol{t}^{\langle\ell\rangle}. \quad (9)$$

It is recalled that, given the spatial variation of the elasticity properties of the layers with respect to the coordinates x_1 and x_2, the matrices $\boldsymbol{Q}_{\lambda\mu}$, $\boldsymbol{R}_{\lambda 3}$ and $\boldsymbol{S}_{33}$ are functions of x_1 and x_2. Finally, upon using integration by parts in Eq.(7), it can be shown that the behavior of VAT multilayered plate is governed by the following system of partial differential equations

$$-\frac{\partial}{\partial x_\lambda} \left(\boldsymbol{Q}_{\lambda\mu} \frac{\partial \boldsymbol{U}}{\partial x_\mu} + \boldsymbol{R}_{\lambda 3} \boldsymbol{U} \right) + \boldsymbol{R}_{\lambda 3}^\intercal \frac{\partial \boldsymbol{U}}{\partial x_\lambda} + \boldsymbol{S}_{33} \boldsymbol{U} = \overline{\boldsymbol{B}}, \quad \text{in } \Omega, \quad (10)$$

subject to the following set of boundary conditions

$$\begin{cases} n_\lambda \left(\boldsymbol{Q}_{\lambda\mu} \frac{\partial \boldsymbol{U}}{\partial x_\mu} + \boldsymbol{R}_{\lambda 3} \boldsymbol{U} \right) = \overline{\boldsymbol{T}}, & \text{on } \partial\Omega_N \\ \boldsymbol{U} = \overline{\boldsymbol{U}}, & \text{on } \partial\Omega_D \end{cases}, \quad (11)$$

where n_λ is the λ-th component of the outward unit normal of the boundary $\partial\Omega$, $\partial\Omega_D \subset \partial\Omega$ is the part of the boundary where the functions $\boldsymbol{U}$ are prescribed, and $\partial\Omega_N \subset \partial\Omega$ is the part of the boundary where the tractions $\boldsymbol{t}$, and consequently $\boldsymbol{T}$, are prescribed. The boundary conditions in Eq.(11) assume that the boundary $\partial\Omega_D$ or $\partial\Omega_N$ is the same for all the functions $\boldsymbol{U}$. However, in general $\partial\Omega_D$ or $\partial\Omega_N$ can be different for each functions contained in $\boldsymbol{U}$ but this aspect does not represent a restriction for the formulation.

The numerical solution of Eqs.(10) and (11) by means of the discontinuous Galerkin approach is discussed in the next section.

3 DISCONTINUOUS GALERKIN FORMULATION

Within the dG framework, an auxiliary flux variable is introduced into the problem and the governing equations are transformed into a first-order system of partial differential equations [12]. In this case, given the specific form of Eqs.(10) and (11), it is convenient to define the flux $\boldsymbol{\Sigma}_\lambda \equiv \boldsymbol{Q}_{\lambda\mu}\frac{\partial \boldsymbol{U}}{\partial x_\mu} + \boldsymbol{R}_{\lambda 3}$, where it is recalled that $\lambda, \mu = 1, 2$, and to rewrite Eq.(10) as follows

$$-\frac{\partial \boldsymbol{\Sigma}_\lambda}{\partial x_\lambda} + \boldsymbol{R}_{\lambda 3}^\intercal \frac{\partial \boldsymbol{U}}{\partial x_\lambda} + \boldsymbol{S}_{33}\boldsymbol{U} = \overline{\boldsymbol{B}} \tag{12a}$$

$$\boldsymbol{\Sigma}_\lambda = \boldsymbol{Q}_{\lambda\mu}\frac{\partial \boldsymbol{U}}{\partial x_\mu} + \boldsymbol{R}_{\lambda 3}\boldsymbol{U}. \tag{12b}$$

The equations given in (12a) and (12b) are then stated in weak sense over a generic subset $\Omega^{(e)}$ of the entire domain Ω. In the numerical applications, $\Omega^{(e)}$ basically represents the generic element of a suitably introduced mesh of Ω. In what follows, quantities referred to the e-th mesh element will be denoted using the superscript (e).

Let us suppose that the domain Ω is divided into N_e non-overlapping elements, i.e. $\Omega = \bigcup_{e=1}^{N_e} \Omega^{(e)}$, and let us introduce the space $\mathcal{V}_h$ of discontinuous polynomials defined as

$$\mathcal{V}_h \equiv \{v : \Omega \to \mathbb{R} \mid v|_{\Omega^{(e)}} \in \mathcal{Q}_p^{(e)} \ \forall e = 1, \dots, N_e\}$$

where $\mathcal{Q}_p^{(e)}$ is the space of the polynomials functions of degree $p \geq 1$ on $\Omega^{(e)}$. Accordingly, we define the space $\mathcal{V}_h^d$ of discontinuous polynomial vector fields as $\mathcal{V}_h^d \equiv (\mathcal{V}_h)^d$.

The weak form of Eqs.(12a) and (12b) is obtained by introducing the test functions $\boldsymbol{V}, \boldsymbol{\Gamma}_\lambda \in \mathcal{V}_h^{N_u}$, where N_u has been defined in Section (2.2). Upon left-multiplying Eq.(12a) by $\boldsymbol{V}^\intercal$, integrating over the generic element e and using integration by parts, one obtains

$$\int_{\Omega^{(e)}} \frac{\partial \boldsymbol{V}^\intercal}{\partial x_\lambda}\boldsymbol{\Sigma}_{h\lambda} + \boldsymbol{V}^\intercal\left(\boldsymbol{R}_{\lambda 3}^\intercal\frac{\partial \boldsymbol{U}_h}{\partial x_\lambda} + \boldsymbol{S}_{33}\boldsymbol{U}_h\right) = \int_{\partial\Omega^{(e)}} \boldsymbol{V}^\intercal\boldsymbol{\Sigma}_\lambda^\star n_\lambda + \int_{\Omega^{(e)}} \boldsymbol{V}^\intercal\overline{\boldsymbol{B}}, \tag{13}$$

where $\partial\Omega^{(e)}$ represents the boundary of $\Omega^{(e)}$. The weak form of Eq.(12b) is instead given by writing

$$\int_{\Omega^{(e)}} \boldsymbol{\Gamma}_\lambda^\intercal\boldsymbol{\Sigma}_{h\lambda} = \int_{\Omega^{(e)}} \boldsymbol{\Gamma}_\lambda^\intercal\left(\boldsymbol{Q}_{\lambda\mu}\frac{\partial \boldsymbol{U}_h}{\partial x_\mu} + \boldsymbol{R}_{\lambda 3}\boldsymbol{U}_h\right) + \int_{\partial\Omega^{(e)}} (\boldsymbol{\Gamma}_\lambda^\intercal\boldsymbol{Q}_{\lambda\mu} + \boldsymbol{V}^\intercal\boldsymbol{R}_{\mu 3}^\intercal)(\boldsymbol{U}^\star - \boldsymbol{U}_h)n_\mu. \tag{14}$$

A few remarks follow: *i*) in Eqs.(13) and (14), $\boldsymbol{U}^\star$ and $\boldsymbol{\Sigma}^\star_\lambda$ denote the *numerical fluxes*, which are approximation of $\boldsymbol{U}$ and $\boldsymbol{\Sigma}_\lambda$, respectively, on the boundary $\partial\Omega^{(e)}$. The specific definition of the numerical fluxes is crucial in the development of a dG method as it leads to different dG formulations and affects the stability and accuracy of the method as well as the sparsity pattern of the resulting stiffness matrix [12]. *ii*) the specific form of Eq.(14) has been chosen to obtain a symmetric dG formulation that verifies the *consistency* condition as it will be shown in Section (3.1). *iii*) in Eqs.(13) and (14), the symbols $\boldsymbol{U}_h$ and $\boldsymbol{\Sigma}_{h\lambda}$ denote the solutions of the weak form of the governing equations and are approximations of $\boldsymbol{U}$ and $\boldsymbol{\Sigma}_\lambda$ appearing in Eqs.(12a) and (12b).

The dG formulation for the whole domain is obtained by summing Eqs.(13) and (14) over the elements of the mesh and by giving the explicit expressions of the numerical fluxes. Let us define $\partial\Omega^{(e)}_I$ as the subset of $\partial\Omega^{(e)}$ that the e-th element shares with the neighboring elements and $\partial\Omega^{(e)}_D$ and $\partial\Omega^{(e)}_N$ as the subsets of $\partial\Omega^{(e)}$ where the Dirichlet boundary conditions and the Neumann boundary conditions, respectively, are enforced. It is clear that given the location of the element inside the mesh, some of the above sets might be empty. Moreover, let $\partial\Omega_I$ be the union of all the $\partial\Omega^{(e)}_I$, i.e. $\partial\Omega_I \equiv \bigcup_e \partial\Omega^{(e)}_I$, and, consistently, $\partial\Omega_D$ and $\partial\Omega_N$, which have been introduced in Section (2.2), are $\partial\Omega_D \equiv \bigcup_e \partial\Omega^{(e)}_D$ and $\partial\Omega_N \equiv \bigcup_e \partial\Omega^{(e)}_N$, respectively. It is worth noting that $\partial\Omega_I$ can also be identified as the union of all the *internal* edges of the mesh, that is $\partial\Omega_I = \bigcup_i I^{(i)}$, where $I^{(i)}$ denotes the generic i-th interface identified by two neighboring elements $\Omega^{(e)}$ and $\Omega^{(e')}$, i.e. $I^{(i)} = \Omega^{(e)} \cap \Omega^{(e')}$.

Considering the above definitions and summing over the mesh elements, Eqs.(13) and (14) lead to the following equations

$$\sum_e \int_{\Omega^{(e)}} \frac{\partial \boldsymbol{V}^\intercal}{\partial x_\lambda} \boldsymbol{\Sigma}_{h\lambda} + \boldsymbol{V}^\intercal \left(\boldsymbol{R}^\intercal_{\lambda 3} \frac{\partial \boldsymbol{U}_h}{\partial x_\lambda} + \boldsymbol{S}_{33} \boldsymbol{U}_h \right) = \sum_i \int_{I^{(i)}} \{\boldsymbol{V}\}^\intercal [\![\boldsymbol{\Sigma}^\star_\lambda]\!]_\lambda + [\![\boldsymbol{V}]\!]^\intercal_\lambda \{\boldsymbol{\Sigma}^\star_\lambda\} + \\ + \sum_e \int_{\partial\Omega^{(e)}_N \cup \partial\Omega^{(e)}_D} \boldsymbol{V}^\intercal \boldsymbol{\Sigma}^\star_\lambda n_\lambda + \sum_e \int_{\Omega^{(e)}} \boldsymbol{V}^\intercal \overline{\boldsymbol{B}} \quad (15)$$

and

$$\sum_e \int_{\Omega^{(e)}} \boldsymbol{\Gamma}^\intercal_\lambda \boldsymbol{\Sigma}_{h\lambda} = \sum_e \int_{\Omega^{(e)}} \boldsymbol{\Gamma}^\intercal_\lambda \left(\boldsymbol{Q}_{\lambda\mu} \frac{\partial \boldsymbol{U}_h}{\partial x_\mu} + \boldsymbol{R}_{\lambda 3} \boldsymbol{U}_h \right) + \\ + \sum_i \int_{I^{(i)}} \{\boldsymbol{\Gamma}^\intercal_\lambda \boldsymbol{Q}_{\lambda\mu} + \boldsymbol{V}^\intercal \boldsymbol{R}^\intercal_{\mu 3}\} [\![\boldsymbol{U}^\star - \boldsymbol{U}_h]\!]_\mu + [\![\boldsymbol{\Gamma}^\intercal_\lambda \boldsymbol{Q}_{\lambda\mu} + \boldsymbol{V}^\intercal \boldsymbol{R}^\intercal_{\mu 3}]\!]_\mu \{\boldsymbol{U}^\star - \boldsymbol{U}_h\} + \\ + \sum_e \int_{\partial\Omega^{(e)}_N \cup \partial\Omega^{(e)}_D} (\boldsymbol{\Gamma}^\intercal_\lambda \boldsymbol{Q}_{\lambda\mu} + \boldsymbol{V}^\intercal \boldsymbol{R}^\intercal_{\mu 3})(\boldsymbol{U}^\star - \boldsymbol{U}_h) n_\mu, \quad (16)$$

respectively. In Eqs.(15) and (16), the following *average* and *jump* operators have been introduced

$$\{\bullet\}^{(i)} = \frac{1}{2} \left(\bullet^{(e)} + \bullet^{(e')} \right) \quad \text{and} \quad [\![\bullet]\!]^{(i)}_\lambda = n^{(e)}_\lambda \, \bullet^{(e)} + n^{(e')}_\lambda \bullet^{(e')}, \quad (17)$$

which are defined for each couple of neighboring elements e and e' sharing the interface i. It is worth noting that in Eqs.(15) and (16), the superscripts (e) and (i) have been dropped as the dependence of the integrand quantities is clear from the domains of integration.

To complete the dG formulation, the numerical fluxes $\boldsymbol{U}^\star$ and $\boldsymbol{\Sigma}^\star_\lambda$ need to be explicitly given in terms of the unknown functions $\boldsymbol{U}_h$ and their derivatives $\partial \boldsymbol{U}_h/\partial x_\lambda$ [12]. In this work, an Interior Penalty (IP) discontinuous Galerkin method is proposed and its implementation is discussed next.

3.1 Interior Penalty formulation

In the proposed IP discontinuous Galerkin method for multilayered VAT plate theories, the numerical fluxes are chosen as follows

$$\boldsymbol{U}^\star = \begin{cases} \{\boldsymbol{U}_h\}, & \text{on } I^{(i)} \\ \overline{\boldsymbol{U}}, & \text{on } \partial\Omega_D^{(e)} \\ \boldsymbol{U}_h, & \text{on } \partial\Omega_N^{(e)} \end{cases} \tag{18}$$

and

$$\begin{cases} \boldsymbol{\Sigma}^\star_\lambda = \{\boldsymbol{Q}_{\lambda\mu}\frac{\partial \boldsymbol{U}_h}{\partial x_\mu} + \boldsymbol{R}_{\lambda 3}\boldsymbol{U}_h\} - \mu[\![\boldsymbol{U}_h]\!]_\lambda, & \text{on } I^{(i)} \\ \boldsymbol{\Sigma}^\star_\lambda = \boldsymbol{Q}_{\lambda\mu}\frac{\partial \boldsymbol{U}_h}{\partial x_\mu} + \boldsymbol{R}_{\lambda 3}\boldsymbol{U}_h - \mu(\boldsymbol{U}_h - \overline{\boldsymbol{U}})n_\lambda, & \text{on } \partial\Omega_D^{(e)} \\ n_\lambda \boldsymbol{\Sigma}^\star_\lambda = \overline{\boldsymbol{T}}, & \text{on } \partial\Omega_N^{(e)} \end{cases}, \tag{19}$$

where μ denotes the penalty parameter.

Setting $\boldsymbol{\Gamma}_\lambda \equiv \partial \boldsymbol{V}/\partial x_\lambda$, and substituting the expression of the numerical fluxes given in Eqs.(18) and (19), Eqs.(15) and (16) can be combined to obtain the *primal form* of the proposed IP dG as follows

$$B_{\mathtt{IP}}(\boldsymbol{V}, \boldsymbol{U}_h) = R_{\mathtt{IP}}(\boldsymbol{V}, \overline{\boldsymbol{B}}, \overline{\boldsymbol{T}}, \overline{\boldsymbol{U}}), \tag{20}$$

where

$$\begin{aligned} B_{\mathtt{IP}}(\boldsymbol{V}, \boldsymbol{U}_h) = &\sum_e \int_{\Omega^{(e)}} \frac{\partial \boldsymbol{V}^\intercal}{\partial x_\lambda}\left(\boldsymbol{Q}_{\lambda\mu}\frac{\partial \boldsymbol{U}_h}{\partial x_\mu} + \boldsymbol{R}_{\lambda 3}\boldsymbol{U}_h\right) + \boldsymbol{V}^\intercal\left(\boldsymbol{R}^\intercal_{\lambda 3}\frac{\partial \boldsymbol{U}_h}{\partial x_\lambda} + \boldsymbol{S}_{33}\boldsymbol{U}_h\right) + \\ &- \sum_i \int_{I^{(i)}} [\![\boldsymbol{V}]\!]^\intercal_\lambda \left\{\boldsymbol{Q}_{\lambda\mu}\frac{\partial \boldsymbol{U}_h}{\partial x_\mu} + \boldsymbol{R}_{\lambda 3}\boldsymbol{U}_h\right\} + \left\{\frac{\partial \boldsymbol{V}^\intercal}{\partial x_\lambda}\boldsymbol{Q}_{\lambda\mu} + \boldsymbol{V}^\intercal\boldsymbol{R}^\intercal_{\mu 3}\right\}[\![\boldsymbol{U}_h]\!]_\mu + \\ &- \sum_e \int_{\partial\Omega_D^{(e)}} n_\lambda \boldsymbol{V}^\intercal\left(\boldsymbol{Q}_{\lambda\mu}\frac{\partial \boldsymbol{U}_h}{\partial x_\mu} + \boldsymbol{R}_{\lambda 3}\boldsymbol{U}_h\right) + \left(\frac{\partial \boldsymbol{V}^\intercal}{\partial x_\lambda}\boldsymbol{Q}_{\lambda\mu} + \boldsymbol{V}^\intercal\boldsymbol{R}^\intercal_{\mu 3}\right)\boldsymbol{U}_h n_\mu + \\ &+ \sum_i \int_{I^{(i)}} \mu[\![\boldsymbol{V}]\!]^\intercal_\lambda[\![\boldsymbol{U}_h]\!]_\lambda + \sum_e \int_{\partial\Omega_D^{(e)}} \mu \boldsymbol{V}^\intercal\boldsymbol{U}_h \end{aligned} \tag{21}$$

and

$$\begin{aligned} R_{\mathtt{IP}}(\boldsymbol{V}, \overline{\boldsymbol{B}}, \overline{\boldsymbol{T}}, \overline{\boldsymbol{U}}) = &\sum_e \int_{\Omega^{(e)}} \boldsymbol{V}^\intercal\overline{\boldsymbol{B}} + \sum_e \int_{\partial\Omega_N^{(e)}} \boldsymbol{V}^\intercal\overline{\boldsymbol{T}} + \\ &- \sum_e \int_{\partial\Omega_D^{(e)}} \left(\frac{\partial \boldsymbol{V}^\intercal}{\partial x_\lambda}\boldsymbol{Q}_{\lambda\mu} + \boldsymbol{V}^\intercal\boldsymbol{R}^\intercal_{\mu 3}\right)\overline{\boldsymbol{U}} n_\mu + \sum_e \int_{\partial\Omega_D^{(e)}} \mu \boldsymbol{V}^\intercal\overline{\boldsymbol{U}}. \end{aligned} \tag{22}$$

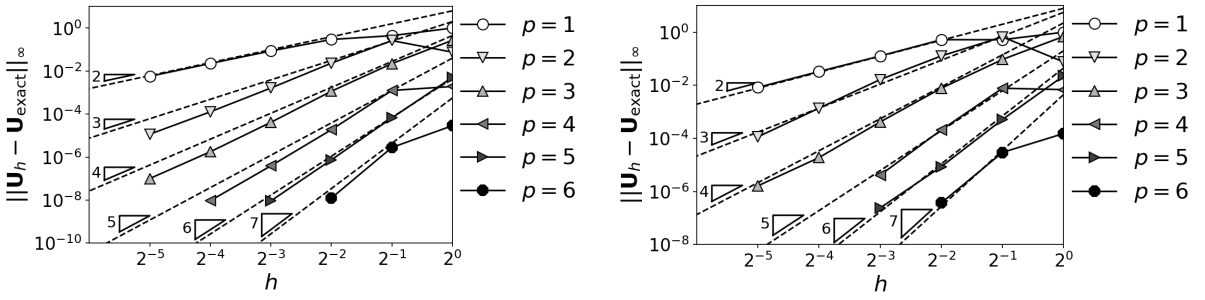

(a) (b)

Figure 2: *hp*-convergence analyses for (a) the FSDT and (b) the ED_{222} theory.

It is worth noting that the obtained bilinear form $B_{\text{IP}}(\bullet, \bullet)$ is symmetric and verifies the consistency condition, which ensures the Galerkin orthogonality property, i.e.

$$B_{\text{IP}}(\boldsymbol{V}, \boldsymbol{U} - \boldsymbol{U}_h) = 0, \quad \forall \boldsymbol{V} \in \mathcal{V}_h^{N_u},$$

where $\boldsymbol{U}$ is the exact solution of Eqs.(10) and (11).

4 NUMERICAL RESULTS

In this work, the performance of developed formulation is assessed by considering the composite structure analysed in Ref.[13] and consisting of a two-layer square plate clamped on all its four edges, which are $a = 1$ m long. The two layers have thickness $\tau^{\langle 1 \rangle} = \tau^{\langle 2 \rangle} = 0.05$ m and thus the plate has a total thickness $\tau = 0.1$ m. The plate is referred to a global reference system $x_1 x_2 x_3$ located at the center of the plate midplane such that the plate occupies the volume $V = [-a/2, a/2] \times [-a/2, a/2] \times [-\tau/2, \tau/2]$ and the modeling plane is $\Omega = [-a/2, a/2] \times [-a/2, a/2]$. In the following, the layers $\langle \ell \rangle = 1$ and $\langle \ell \rangle = 2$ are referred to as the bottom and top layers, respectively. Two cases of fiber orientation are considered: in the first case, straight fibers are considered and the bottom and top layers have orientation $\theta^{\langle 1 \rangle} = \pi/2$ and $\theta^{\langle 2 \rangle} = 0$, respectively; in the second case, variable angle fibers are considered and the bottom and top layers have orientation $\theta^{\langle 1 \rangle}(x_1, x_2) = (\pi/2)(1 - |x_1/a|)$ and $\theta^{\langle 2 \rangle} = (\pi/2)|x_1/a|$, respectively. For all the considered plate theories, a Taylor expansion of the displacement components is assumed, whereas Legendre polynomials are chosen as test and trial functions.

The *hp*-convergence of the proposed formulation is investigated by setting the right-hand side $\overline{\boldsymbol{B}}$ so that the exact solution of the governing equations given in Eq.(10) has the expression $\boldsymbol{U}_{\text{exact}} = \boldsymbol{U}_0 \sin(\pi x_1/a) \sin(\pi x_2/a)$, where $\boldsymbol{U}_0$ is a constant vector with components equal to 1. The straight-fiber structure is considered in this case and the properties of the orthotropic material are chosen in an adimensionalized fashion as $E_{11} = 25$, $E_{22} = E_{33} = 1$, $G_{23} = 0.2$, $G_{12} = G_{13} = 0.5$ and $\nu_{23} = \nu_{12} = \nu_{13} = 0.25$. The selected mesh is a Cartesian grid with square elements of size h and the penalty parameter μ is chosen as $\mu = 125/h$.

Figure (2a) shows the *hp*-convergence results when the First Shear Deformation Theory is selected for the through-the-thickness behavior of the plate. Using the notation

introduced by Demasi, see e.g. [11], the FSDT is referred to as the ED_{110} theory where the E denotes the adoption of the ESL approximation, the D denotes the use of the PVD and the three subscripts denote the order of approximation for the three components of displacement. Referring to the same notation, Fig.(2b) shows the *hp*-convergence results when the ED_{222} theory is selected for the through-the-thickness behavior of the plate. Both figures show the accuracy of the proposed formulation in terms of the effect of the order p of polynomials as well as the effect of the mesh size h on the error $||\boldsymbol{U}_h - \boldsymbol{U}_{\text{exact}}||_\infty$, which is defined as the maximum value among the components of $\boldsymbol{U}_h$ over Ω.

The proposed formulation is then employed to compute the mechanical response in terms of displacement field $\boldsymbol{u}$ of the considered structure under the action of uniform pressure $p = -10$ kPa over the top surface. It is recalled that $\boldsymbol{u}$ is obtained from the unknown functions $\boldsymbol{U}_h$ using Eq.(6). In this case, the properties of the considered orthotropic material are taken from Ref.[13] and are $E_{11} = 137.9$ GPa, $E_{22} = E_{33} = 8.96$ GPa, $G_{23} = 6.21$ GPa, $G_{12} = G_{13} = 7.1$ GPa, $\nu_{23} = 0.49$ and $\nu_{12} = \nu_{13} = 0.3$.

Figures (3a), (3c) and (3e) show the converged values of the displacement components u_1 and u_2 and u_3, respectively, evaluated at $(x_1, x_2) = (-a/2, -a/2)$ as a function of the through-the-thickness variable x_3 for three different selected theories, namely FSDT, ED_{222} and ED_{444}, in case of the straight-fiber structure. Similarly, Figs.(3b), (3d) and (3f) show the displacement components u_1 and u_2 and u_3, respectively, in case of the VAT structure. Moveover, the figures shows the comparison of the results obtained with the present dG formulation with those obtained using fourth-order triangular finite elements and available in Ref.[13] when the ED_{444} theory is selected. It is worth noting that the satisfactory level of accuracy shown in the figures is obtained with $h = 1/4$, i.e. 16 elements, and $p = 8$ that corresponds to a total number of 19440 degrees of freedom, which is less than half the number of degrees of freedom using finite elements [13].

5 CONCLUSIONS

In this work, an Interior Penalty discontinuous Galerkin formulation for the mechanical behaviour of VAT multi-layered composite plates has been presented. The formulation has been developed starting from the strong form of the governing equations of general higher-order theories of VAT plates based on the Principle of Virtual Displacement, the Generalized Unified Formulation and the Equivalent Single Layer Assumption for the behavior of the plate assembly. Upon introducing an auxiliary flux variable and suitably defined average and jump operators, the weak form of the governing equations has been written within the discontinuous Galerkin framework and, subsequently, the explicit expressions of the numerical fluxes have defined the proposed Interior Penalty formulation. The presented numerical results show the accuracy of the method as well as the computational savings in terms of degrees of freedom with respect to finite element approaches.

6 ACKNOWLEDGMENTS

The authors gratefully acknowledge the support of CINECA's staff for the use of CINECA's HPC facilities.

REFERENCES

[1] Jones, R.M. *Mechanics of composite materials.* CRC press, 1998

[2] Gurdal, Z., and Olmedo, R. In-plane response of laminates with spatially varying fiber orientations-variable stiffness concept *AIAA J.* (1993) **31**:751–758.

[3] Biggers, S.B., and Pageau, S.S., Shear buckling response of tailored composite plates *AIAA J.* (1994) **32**:1100–1103.

[4] Oliveri, V. and Milazzo, A. A Rayleigh-Ritz approach for postbuckling analysis of variable angle tow composite stiffened panels *Comput. Struct.* (2018) **196**:263–276.

[5] Oliveri, V., Milazzo, A. and Weaver, P.M. Thermo-mechanical post-buckling analysis of variable angle tow composite plate assemblies *Compos. Struct.* (2018) **183**:620–635.

[6] Wu, Z., Raju, G., and Weaver, P.M. Framework for the buckling optimization of variable-angle tow composite plates *AIAA J.* (2015) **53**:3788–3804.

[7] Saye, R. Implicit mesh discontinuous Galerkin methods and interfacial gauge methods for high-order accurate interface dynamics, with applications to surface tension dynamics, rigid body fluid–structure interaction, and free surface flow: Part I *J. Comput. Phys.* (2017) **344**:647–682.

[8] Carrera, E. and Demasi, L. Classical and advanced multilayered plate elements based upon PVD and RMVT. Part 1: Derivation of finite element matrices *Int. J. Numer. Meth. Eng.* (2002) **55**:191–231.

[9] Carrera, E. Theories and finite elements for multilayered plates and shells: a unified compact formulation with numerical assessment and benchmarking *Arch. Comput. Meth. Eng.* (2003) **3**:215–296.

[10] Demasi, L., ∞^3 Hierarchy plate theories for thick and thin composite plates: the generalized unified formulation *Compos. Struct.* (2008) **84**:256–270.

[11] Demasi, L., Invariant finite element model for composite structures: The generalized unified formulation *AIAA J.* (2010) **48**:1602–1619.

[12] Arnold, D.N., Brezzi F., Cockburn B. and Marini, L.D. Unified analysis of discontinuous Galerkin methods for elliptic problems *SIAM J. Numer. Anal.* (2002) **39**:1749–1779.

[13] Demasi, L., Biagini, G., Vannucci, F., Santarpia, E., and Cavallaro, R. Equivalent Single Layer, Zig-Zag, and Layer Wise theories for variable angle tow composites based on the Generalized Unified Formulation *Compos. Struct.* (2017) **177**:54–79.

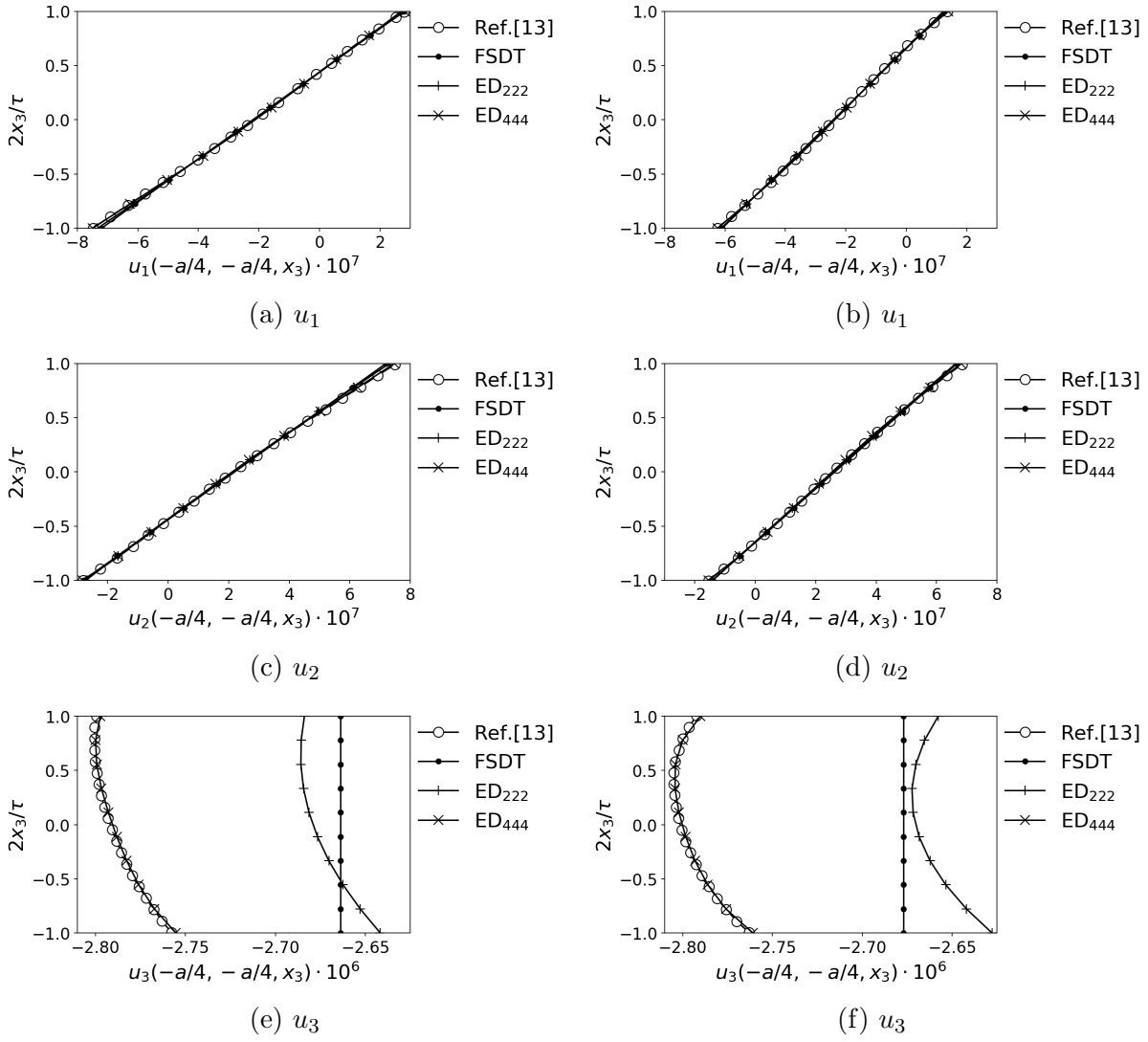

(a) u_1 (b) u_1

(c) u_2 (d) u_2

(e) u_3 (f) u_3

Figure 3: Displacement components evaluated at $(x_1, x_2) = (-a/4, -a/4)$ and computed using three different plate theories as a function of the through-the-thickness variable x_3. Figures (a,c,e) refer to the straight-fiber case whereas Figs.(b,d,f) refer to the VAT case.